KSCE Journal of Civil Engineering (2018) 22(10):3772-3782

DOI 10.1007/s12205-018-1334-6

Environmental Engineering

pISSN 1226-7988, eISSN 1976-3808
www.springer.com/12205

Adsorption Mechanisms of Manganese (II) Ions onto Acid-treated Activated Carbon

Thi Nhung Tran*, Do-Gun Kim, and Seok-Oh Ko*****

Received September 6, 2017/Revised November 20, 2017/Accepted December 11, 2017/Published Online July 7, 2018

In this work, modification of Granular Activated Carbon (GAC) using nitric acid as an oxidizing agent was investigated to develop a novel adsorbent that can effectively remove manganese from aquatic environments. The results revealed that the acid modification method reduced BET surface area, micropore volume, and the point of zero charge (pH_{PZC}) but produced more carboxylic acid groups on the M-GAC surface. Batch adsorption experiment results indicated that pH, adsorbent dosage, initial Mn(II) concentration, and solution temperature dramatically influenced the Mn(II) ions adsorptive behavior. The M-GAC showed maximum adsorption capacity for Mn(II) ions (9.25 mg/g) significantly higher compared to that of R-GAC (1.29 mg/g). Equilibrium data were evaluated by Langmuir, Freundlich, Sips, and Tempkin isotherm models, and the results suggested that the Sips model is the most suitable to expound the adsorption behavior of Mn(II) ions on both M-GAC and R-GAC. The pseudo second order kinetic model exhibited a better fit with the adsorption kinetic data of both M-GAC and R-GAC. The three-stage kinetic model revealed that the enhancement of Mn(II) adsorption on M-GAC was exclusively due to an increase in adsorption on the external and internal surfaces of M-GAC. Also, external mass transfer and intraparticle diffusion were both involved in the rate controlling step of the Mn(II) adsorption onto M-GAC. In addition, the resistance of mass transfer during the adsorption was verified primarily dependent on the external mass transfer via the mass transfer factor model. Overall, the results obtained from this study provides an insight into the adsorption mechanisms of Mn(II) ions onto the acid treated GAC.Abstract

Keywords: *adsorption, equilibrium, kinetic, manganese, surface functional groups, surface modification*

1. Introduction

Manganese is well known as one of the most plentiful elements in our planet's surface, and is a crucial micronutrient for the human body and organisms (Tavlieva *et al.,* 2015). Although the presence of Mn at low concentrations in aqueous systems is not considered to be as ecotoxic as other metals (e.g., Fe, Al, and Zn), excessive Mn concentrations can cause undesirable effects such as blockages within water distribution pipelines, discoloration of laundry, and a metallic taste in drinking water (Emmanuel and Rao, 2009). In addition, prolonged exposure to high Mn concentrations can be toxic for embryos and fetuses and cause DNA damage, respiratory disorders, neurotoxic effects, and even manganism-Parkinson disease (Michalke and Fernsebner, 2014). A concentration of Mn below 0.05 mg/L in drinking water is generally acceptable, which is suggested by the World Health Organization (WHO, 2011). For these reasons, controlling the quantity of manganese in water is of great importance.

Many techniques have been suggested as potential treatment methods to effectively remove soluble Mn, such as filtration, coagulation–flocculation, electrocoagulation, chemical precipitation, adsorption, ion exchange, membrane separation, and biological treatment (Patil *et al.,* 2016). Among them, adsorption has been widely investigated as the most cost-effective and environmentally-friendly method for eliminating metal ions (Rivera-Utrilla *et al.,* 2011). Likewise, Activated Carbon (AC), which possesses high specific surface area, large porosity, excellent internal microporosity, and variety of surface functional groups, has proven to be the most popular adsorbent for separating contaminants during water treatment (Ademiluyi and David-West, 2012). Remarkably, functionalization of the AC surface significantly influences the adsorption behavior of the AC (Yahya *et al.,* 2015). Therefore, modification of surface functional groups is an attractive way to increase the performance of AC for removing specific pollutants (Bhatnagar *et al.,* 2013). Various modification methods have been published in the literature, including acid/ base treatment, ozone, plasma, impregnation, and microwave treatment (Anisuzzaman *et al.,* 2015; ChangMing *et al.,* 2013; Jaramillo *et al.,* 2010; Ahn *et al.,* 2009; Üçer *et al.,* 2006). In this respect, adding acidic functional groups to the AC surface (e.g., carboxyl, carbonyl, carboxylic anhydride, lactone, and hydroxyl) could offer some advantages for removing heavy metals due to their propensity to constitute metal complexes (Gaur and Shankar, 2012). Treatment of AC with nitric acid can also be industrially valuable in terms of cost, time, and operating temperature (ShamsiJazeyi and Kaghazchi, 2010). Although many previous studies have verified

*Ph.D. Student, Dept. of Civil Engineering, Kyung Hee University, Yongin 17104, Korea (E-mail: trannhung@khu.ac.kr)
**Member, Research professor, Dept. of Civil Engineering, Kyung Hee University, Yongin 17104, Korea (E-mail: dogun.kim@khu.ac.kr)
***Member, Professor, Dept. of Civil Engineering, Kyung Hee University, Yongin 17104, Korea (Corresponding Author, E-mail: soko@khu.ac.kr)

that acid-treated AC shows enhanced adsorption capacity, the adsorption mechanisms of this modified AC toward heavy metals have not been clearly investigated.

In this study, we attempted to characterize the physico-chemical properties and surface functional groups of acid-modified GAC. Equilibrium and kinetic experiments investigating Mn(II) adsorption onto unmodified and modified GAC surfaces were conducted. Various equilibrium isotherms and kinetic models were used to examine experimental data in order to obtain a deeper understanding of the adsorption mechanisms. Mn(II) removal under different experimental conditions (e.g., pH, temperature, initial Mn(II) concentration, and adsorbent dose) were conducted to investigate the adsorption behavior. In addition, a desorption experiment was also carried out to assess the capability of the adsorbents to retain Mn(II).

2. Materials and Methods

2.1 Adsorbents Preparation

Granular activated carbon (NORIT® GAC 1240, Norit Americas Inc., USA), was continually rinsed with deionized water (DIW) and nitric acid (69% HNO_3) to remove impurities and reduce the alkalinity until pH around 7.0. Afterward, it was completely dried at 60°C. This dried material is referred to as untreated GAC (R-GAC). A portion of this R-GAC material was then continuously modified with concentrated nitric acid (69% HNO_3). The detailed modification procedure was as follows: a mixture of R-GAC and concentrated R-GAC: HNO_3 = 1: 15, by mass ratio) was put in a four-neck round flask equipped with a magnetic stir bar. The mixture was then gently mixed for 24 h at 50°C. The resultant GAC was collected and subsequently thoroughly rinsed with DIW. To minimize the decomposition of functional groups, the as-prepared GAC was first exposed to room temperature for 1 day and then air-dried at 105°C for 12 h. This acid-modified GAC is referred to as M-GAC. All chemicals and reagents used for this work were supplied by Sigma-Aldrich Corp., USA.

2.2 Characterization of Adsorbents

The morphology of the prepared materials was characterized by field emission scanning electron microscopy (FE-SEM, Leo Supra 55, Genesis 2000, EDAX, Carl Zeiss Corp., Germany) equipped with energy dispersive X-ray spectroscopy (EDX). The Brunauer-Emmett-Teller (BET) specific area, the Barrett-Joyner-Halenda (BJH) pore size distribution and pore volume were analyzed by N_2 adsorption/desorption isotherms method using a BELSORP-max surface analyzer (MicrotracBEL Corp., Japan). The surface functional groups of prepared absorbents were analyzed by Fourier transform infrared (FTIR) spectroscopy using a Spectrum One FTIR spectrometer (Perkin-Elmer, USA) in a spectral region of 4000-450 cm^{-1} and 1 cm^{-1} of resolution. The samples were prepared by a potassium bromide (KBr) pelleting technique. A zeta potential machine (BI-9000AT, Brookhaven Instruments Corp., USA) with dynamic light scattering was employed to define point of zero charge (pH_{PZC}).

2.3 Batch Adsorption Experiments

The adsorption equilibrium experiments were performed via a series of batch experiments by adding 0.1 g of absorbents into conical vials containing 40 mL of Mn(II) solutions (0-120 mg/L), at pH 6.0. These vials were placed in the WIS-20 shaking incubator (DAIHAN Scientific Co., Ltd, Korea) at 25°C and agitated at 150 rpm for 12 h. Adsorption kinetics were studied by suspending 0.5 g of adsorbents into 250 mL Mn(II) solutions (20 mg/L), then proceeded for 180 min. Aliquot samples were collected at given time intervals. Affecting factors, i.e., initial pH (3.0-11.0), temperature (20-40°C), initial Mn(II) concentration (50-200 mg/L), and adsorbent dosage (0.05-0.50 g) toward the adsorption of Mn(II) were investigated via a batch processing for 180 min. To evaluate the sustainability of adsorbed Mn(II) ions onto absorbent surfaces, desorption experiments were accomplished immediately after adsorption process by replacing 20 mL of the equilibrium suspension with the same DIW volume or NaCl with the final concentration of 1.0 M. This process diluted the Mn(II) concentration in the solutions by half, altering the pre-established equilibrium. Subsequently, the solution was shaken for additional 12 h under the same conditions used for the adsorption test. Collected samples were filtered through a polyvinylidene fluoride (PVDF) membranes with pore size of 0.22 μm. The filtrates were adjusted to a pH < 3 by 0.1M HNO_3, then the Mn(II) concentration was monitored by an Inductively Coupled Plasma Mass Spectrometry (ICP-MS) method (OPTIMA 5300 DV, Perkin Elmer, USA). All tests were made in duplicate, and the further results were obtained by calculating the average values from experimental data.

The quantity of adsorbed Mn(II) on a unit mass of R-GAC and M-GAC (q, mg/g) was computed by the following mass balance equation:

$$q = \frac{(C_o - C_e)V}{m} \quad (1)$$

where C_o and C_e (mg/L) are the initial and equilibrium Mn(II) concentrations, respectively; V (L) is the adsorbate volume; and m (g) is the amount of R-GAC or M-GAC used.

2.4 Adsorption Models

2.4.1 Adsorption Isotherms

There are several models that can be used to analyze the experimental data. Here, the Langmuir (Langmuir, 1918), Freundlich (Freundlich, 1906), Sips (Sips, 1948), and Tempkin isotherm (Choy *et al.,* 1999) models were tested.

The linearized and nonlinearized isotherm equations of the Langmuir, Freundlich, Sips, and Tempkin models are given in Table 1, where q_e is the quantity of Mn(II) adsorbed on a unit mass of R-GAC or M-GAC (mg/g), q_{max} is the maximum adsorption capacity (mg/g), C_e is the equilibrium concentration of Mn(II) (mg/L), K_L is the Langmuir adsorption constant (L/mg), K_F is the Freundlich constant (mg/g (L/mg)$^{1/n}$), $1/n$ is a

Table 1. Equilibrium Models Used to Investigate Mn(II) Adsorption onto R-GAC and M-GAC

Isotherm model	Nonlinear form	Linear form
Langmuir	$q_e = q_{\max}\frac{K_L C_e}{1+K_L C_e}$	$\frac{1}{q_e}=\frac{1}{q_{\max}K_L}\frac{1}{C_e}+\frac{1}{q_{\max}}$
Freundlich	$q_e = K_F C_e^{1/n}$	$\log q_e = \frac{1}{n}\log C_e + \log K_F$
Tempkin	$q_e = \frac{RT}{b_T} ln\, A_T C_e$	$q_e = \frac{RT}{b_T} ln C_e + \frac{RT}{b_T} ln\, A_T$
Sips	$q_e = q_{max}\frac{K_S C_e^{n_s}}{1+K_S C_e^{n_s}}$	$\frac{1}{q_e}=\frac{1}{q_{max}K_s}(\frac{1}{C_e})^{n_s}+\frac{1}{q_{max}}$

measurement of the adsorption intensity, R is the gas constant (8.314 J/mol K), T is the absolute temperature (K), b_T is the Tempkin constant associated to the heat of adsorption (J/mol), A_T is the Tempkin equilibrium constant (L/mg), n_s is the Sips model exponent of the adsorbent, and K_s is the Sips constant (1/mg).

2.4.2 Adsorption Kinetics

Experimental kinetic data was analyzed using the pseudo first order, pseudo second order, intraparticle diffusion, the lately advanced three-stage model and the mass transfer factor model. The pseudo first order model supposes that the rate of the adsorption from liquid solution onto adsorbent surface depends proportionally on the disparity in saturated concentration of solute and the adsorbent amount (Belaid *et al.,* 2013). Meanwhile, the pseudo second order kinetic model assumes that the rate controlling step is chemisorption, where the solute is removed due to physico-chemical interplays between the adsorbent and bulk solution (Robati, 2013). The linearized equations of the pseudo first and second order models are described in Eq. (2) and Eq. (3), respectively:

$$\log(q_e - q_t) = \log q_e - \frac{k_1}{2.303}t \tag{2}$$

$$\frac{t}{q_t}=\frac{1}{k_2 q_e^2}+\frac{1}{q_e}t \tag{3}$$

where q_e and q_t are the adsorption capacity of Mn(II) (mg/g) at equilibrium conditions and at contact time t (min), respectively; k_1 (1/min) and k_2 (g/mg min) are the pseudo first order and pseudo second order rate constant, respectively.

To evaluate the role of intraparticle diffusion in the system, the kinetic data are fitted using the model offered by Weber and Morris (1993), which is presented as Eq. (4):

$$q_t = k_{id}t^{0.5} + I \tag{4}$$

where q_t (mg/g) is the adsorption capacity at time t (min), I (intercept) is an arbitrary constant, and k_{id} (mg/g min$^{0.5}$) is the rate constant. If q_t against $t^{0.5}$ plot is linear, intraparticle diffusion is the rate controlling step.

The three-stage model considers three different adsorption stages (Choi *et al.,* 2007). In this model, the first (sharper) portion reflects the instantaneous adsorption of Mn(II) onto the external surface; the second (gradual) portion represents the internal surface adsorption where the dominant mechanism controlling the process is intraparticle diffusion; and the third (constant) portion denotes the equilibrium stage (ShamsiJazeyi and Kaghazchi, 2010). The model equations are expressed as follows:

$$\frac{C_t}{C_o}=\frac{(1-\xi_1)(1-\xi_1-\beta\xi_2)}{(1-\xi_1-\beta\xi_2 e^{-\gamma t})} \tag{5}$$

$$\xi_1=\frac{mq_1(\infty)}{VC_o} \tag{6}$$

$$\xi_2=\frac{mq_2(\infty)}{VC_o} \tag{7}$$

$$\gamma=\frac{(1-\xi_1-\beta\xi_2)\alpha}{\beta\xi_2} \tag{8}$$

where C_t/C_0 is the relative aqueous concentration, and $q_1(\infty)$ and $q_2(\infty)$ are the adsorption capacity for the instantaneous adsorption and the interior sites at infinite time, respectively. ξ_1 is the ratio between the quantity of the adsorbate adsorbed onto the external surface at infinite time and the total quantity of the initial adsorbate. ξ_2 is defined similar to ξ_1; however, it is computed for adsorption into the interior adsorptive sites. α is the rate constant, and β is a limiting factor for $q_2(\infty)$ ($0 < \beta \leq 1$).

The Mass Transfer Factor (MTF) model supposes three successive steps for the adsorption, i.e., (i) external/ film mass transfer, (ii) internal mass transfer/ porous diffusion, (iii) fixation (Fulazzaky *et al.*, 2013, Fulazzaky, 2011). It is able to determine the resistance of mass transfer through the identification of the mass transfer factors, such as Global Mass Transfer (GMT), External Mass Transfer (EMT) and Internal Mass Transfer (IMT) factors. The model equations are described as follows:

$$\ln\left(\frac{C_t}{C_o}\right) = [k_L a]_g e^{-\delta q}t \tag{9}$$

$$q_t = \frac{1}{\delta}\ln(t) + B \tag{10}$$

$$B = \frac{\ln([k_L a]_g) - \ln\left\{\ln\left(\frac{C_o}{C_t}\right)\right\}}{\delta} \tag{11}$$

$$[k_L a]_f = [k_L a]_g e^{-\delta q_t} \tag{12}$$

$$[k_L a]_d = [k_L a]_g - [k_L a]_f \tag{13}$$

where $[k_L a]_g$, $[k_L a]_f$ and $[k_L a]_d$ (1/min) are the GMT, EMT and IMT factors, respectively; q_t (mg/g) is the accumulative amount of Mn(II) ions on the adsorbents at time t (min), δ (g min/mg) is the adsorbate-adsorbent affinity parameter and B (mg/g) is the potential mass transfer index.

3. Results and Discussion

3.1 Characterization of Adsorbents

3.1.1 Physico-chemical Properties

The nitrogen adsorption–desorption isotherms were used to evaluate porous characteristics of the prepared materials. For R-GAC and M-GAC, the nitrogen adsorption–desorption isotherms in Fig. 1 exhibited similar type IV curves classified by the International Union of Pure and Applied Chemistry (IUPAC), with hysteresis loops in the relative pressure (P/P_0) region of 0.45 – 1.0, which reflect the property of mesoporous materials (Do *et al.,* 2017). In addition, Table 2 shows that the average pore diameters of R-GAC and M-GAC were determined as 2.14 nm and 2.22 nm, respectively, further confirming that R-GAC and M-GAC have mesoporous structures. The BET specific surface area of M-GAC (945.89 m^2/g) is quite comparable to that obtained from R-GAC (959.99 m^2/g), which indicates that the HNO_3 alteration did not considerably change the porous structure of the GAC. However, a slightly reduction in BET surface area and micropore volume of M-GAC compare to those of R-GAC can be ascribed to the generation of new functional groups at the entrance and interstices of micropores during the acid modification, that

Table 2. Properties of R-GAC and M-GAC

Material	a_{sBET} $(m^2/g)^a$	V_p $(cm^3/g)^b$	V_m $(cm^3/g)^c$	d_p $(nm)^d$	pH_{PZC}
R-GAC	959.99	0.5125	0.1941	2.14	5.2
M-GAC	945.89	0.5259	0.1737	2.22	2.5

[a]BET specific surface area; [b]Total pore volume; [c]Micropore volume; [d]Average pore diameter. V_p is computed as the liquid volume of N_2 at $P/P_0 = 0.990$.

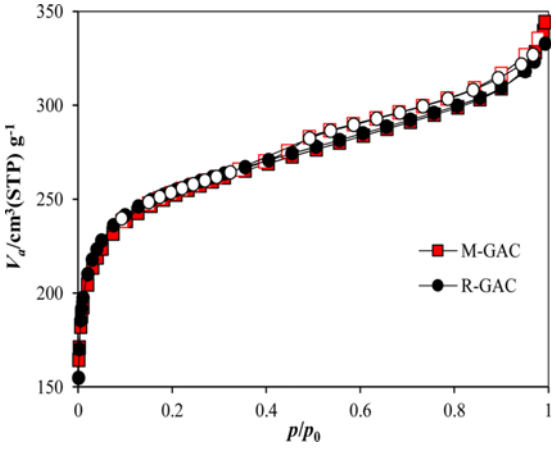

Fig. 1. Typical Nitrogen Adsorption (solid symbols)/desorption (open symbols) Isotherms of R-GAC and M-GAC

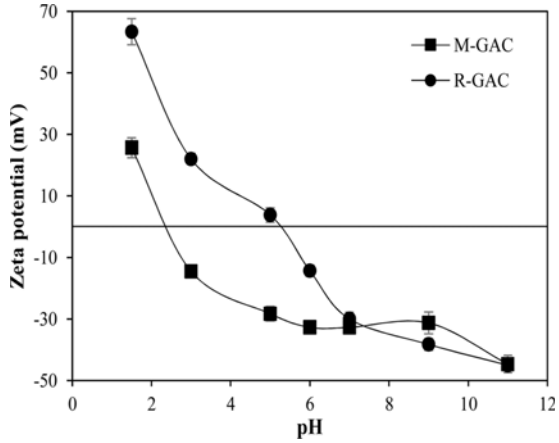

Fig. 2. Zeta Potentials of R-GAC and M-GAC as a Function of pH

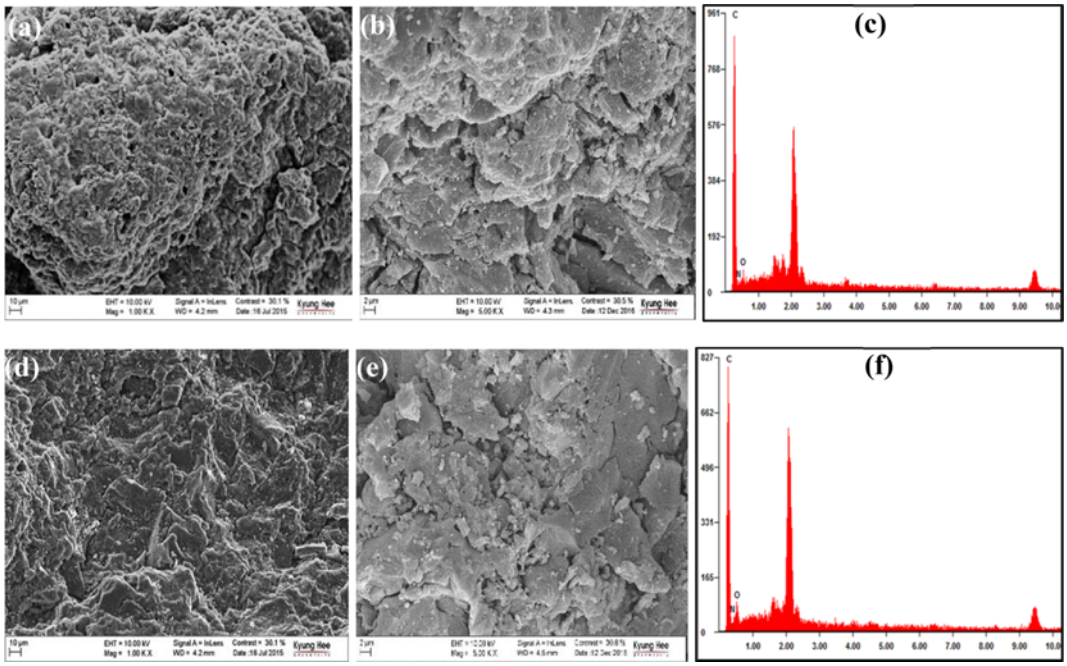

Fig. 3. SEM Images of (a and b) R-GAC and (d and e) M-GAC; EDX Results of (c) R-GAC and (f) M-GAC

tightens the micropores (Zhang *et al.,* 2015).

The zeta potential results for R-GAC and M-GAC are illustrated in Fig. 2. After modification, a significant difference in the point of zero charge (PZC) between M-GAC (pH_{PZC} = 2.5) and R-GAC (pH_{PZC} = 5.2) was obtained. The lower in pHpzc value for M-GAC is reasonable because of an improvement in the number of acidic caborxylic groups on the M-GAC surface after being treated by HNO_3 (Huang *et al.,* 2009). The quantity of acidic functional groups of a material is obviously correlated to the heavy metals adsorption capacity of that material, which suggests that M-GAC might have a greater attraction for metal ions than R-GAC.

The surface morphologies of R-GAC and M-GAC were recorded by SEM/EDX, as illustrated in Fig. 3. It can be seen that the surfaces of both R-GAC and M-GAC are loose and multi-porous; however, M-GAC has a slightly smoother surface than R-GAC.

3.1.2 Changing the Surface Functional Groups

The FTIR of the R-GAC and M-GAC are illustrated in Fig. 4, and the possible band frequencies in the FTIR spectrum of the materials are presented in Table 3. The remarkable increases in the number and relative intensity of peaks between 3500 and 3850 cm^{-1} indicate a significant growth of hydroxyl groups in the carbon surface, which can be ascribed to the enlargement in the number of acidic carboxylic groups (Chen and Wu, 2004). Difference from R-GAC, the bands at 1706 cm^{-1} and 1126 cm^{-1} only appear in the M-GAC spectrum. The band at 1706 cm^{-1} is attributed to the carbonyl groups (C=O), and the band at 1126 cm^{-1} can be caused by both C-O stretching vibration and the O-H bending modes due to the existence of phenolic groups. These results clearly indicate that nitric acid treatment of GAC generates more of these acidic functional groups, which results in the higher Mn(II) uptake compared to that of R-GAC.

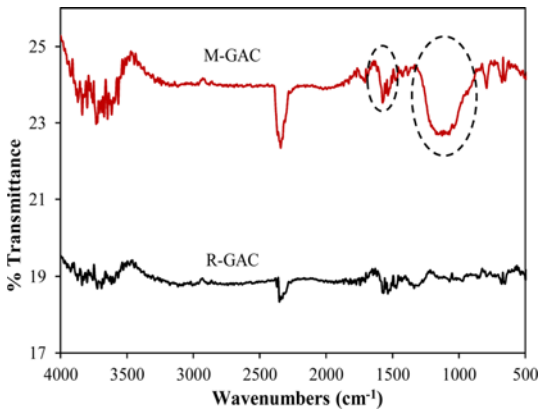

Fig. 4. FTIR Spectra of R-GAC and M-GAC

3.2 Effects of Experimental Parameters

3.2.1 Initial Mn(II) Concentration and Adsorbent Dosage

The effects of initial Mn(II) concentration (50-200 mg/L) and adsorbent dosage (0.05-0.50 g) on adsorption were investigated with a reaction volume of 40 mL at fixed pH (6.0) for 180 min at 25°C. Fig. 5 indicated that the adsorption performance strongly depends on the Mn(II) concentration and the adsorbents dosage. As expected, the adsorption performance of M-GAC was

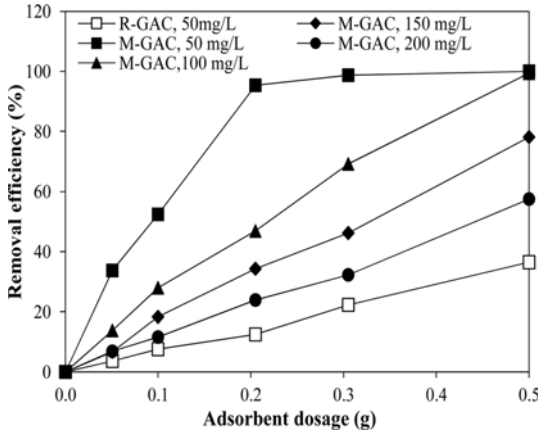

Fig. 5. Effects of Adsorbent Dosage and Initial Mn(II) Concentration on the Adsorption of Mn(II) by R-GAC and M-GAC at 25°C

Table 3. Surface Functional Groups Observed from Absorption Bands in the FTIR Spectra of R-GAC and M-GAC

Functional group	Band position (cm^{-1})		Intensity	Type of Vibration	References
	R-GAC	M-GAC			
O-H	3732	3622, 3723, 3823	strong, sharp	free, stretch (hydroxyl groups)	(Jia and Thomas, 2000; Goel *et al.,* 2005; Huang *et al.*, 2009; ShamsiJazeyi and Kaghazchi, 2010; Yang *et al.*, 2016);
C=O	2352	2342		bend (ketone groups)	
C=O	-	1706	strong	stretch (acid groups)	
C=O	1534, 1568	1534, 1574	strong	stretch (aromatic rings and conjugated carbonyl groups)	
O-H	1336	1338	medium	bend	
C-O	-	1126	strong	stretch (ether, phenol, carboxylic acid, and lactone groups)	
C-O	1070	1072		stretch	
C-H	1471	-	variable	bend	
C-H	-	791	strong	bend	
C-H deformation	653, 677	652, 675	strong		

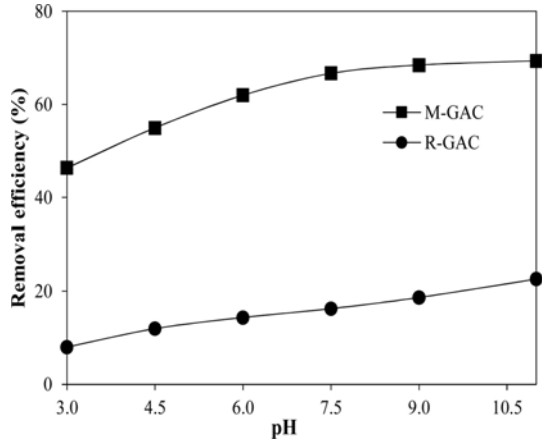

Fig. 6. Effect of pH on the Adsorption of Mn(II) by R-GAC and M-GAC at 25°C

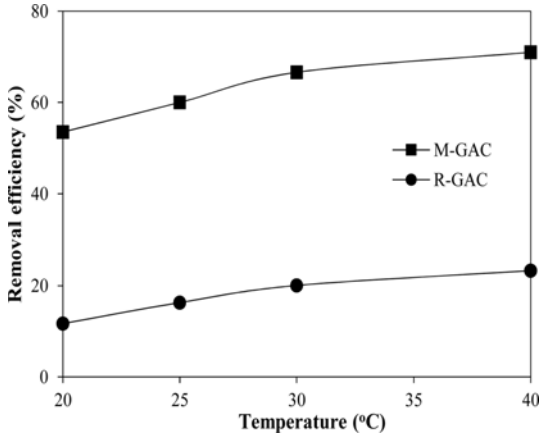

Fig. 7. Effect of Solution Temperature on the Adsorption of Mn(II) by R-GAC and M-GAC

reduced with a rise in initial Mn(II) concentration, because of the shortage of adsorptive sites needed for high levels of Mn(II). In this respect, the uptake of Mn(II) improved with a rise in the adsorbent dosage, especially for M-GAC, which is due to the greater number of adsorptive sites are provided at higher adsorbent dosage. These results also showed that the M-GAC can adsorb Mn(II) more efficiently from the aqueous solution than R-GAC. Considering the removal efficiency, the optimal M-GAC dosage for an Mn(II) concentration of 50 mg/L should be maintained at 0.2 g (i.e., 5 g/L).

3.2.2 pH

pH effect on the adsorption behavior was examined by adding 0.2 g M-GAC or 0.5 g R-GAC into reactors containing 40 mL of 100 mg/L Mn(II) solution at various pH range from 3.0 to 11.0. Figure 6 shows that the adsorbed Mn(II) increased with increasing pH from 3.0 to 7.5, and remains almost constant up to a pH of 11.0 in both M-GAC and R-GAC. Also, we observed that the pH values markedly affect the Mn(II) adsorption capacity of R-GAC (i.e., 12.5% and 42.6% at pH 3.0 and 11.0, respectively) but show only a slight influence on M-GAC (i.e., 91.2% and 99.6% at pH 3.0 and 11.0, respectively). These results can be attributed to the finding that the pH_{PZC} values of M-GAC and R-MAC are 2.5 and 5.2, respectively, indicating that the surfaces of these adsorbents are positively charged at pHs below 2.5 and 5.2, which has an adverse effect to the adsorption of Mn(II) when investigate pH lower than pH_{pzc} values. Additionally, the precipitation of manganese species started at pH 7.75, which could contribute to the increased Mn(II) adsorption efficiency (Li *et al.,* 2010). Furthermore, it is well known that metal cations will compete with protons to bind the adsorption sites on adsorbent surfaces at low pH, resulting in the decrease of adsorption capacity (Zhang *et al.,* 2015).

3.2.3 Temperature

Temperature effect on the uptake of Mn(II) was investigated by employing batch experiment under varying temperature from 20 to 40°C with a designated M-GAC or R-GAC dosage of 0.2 g or 0.5 g, respectively, under a reactor volume of with 40 mL of 100 mg/L Mn(II), at pH 6.0. Fig. 7 shows that the adsorption performance of Mn(II) rised proportionally with the increase of temperature for both M-GAC and R-GAC, implying that this is an endothermic adsorption. Here, the increase in Mn(II) uptake might result from the finding that the hydration shell of metal ions is more effortlessly interrupted as well as the mobility of metal ions increase as the Brownian movement enhancement at a higher temperature, which promotes the diffusion of Mn (II) through the exterior boundary and the interior pores (Kim *et al.,* 2016).

3.3 Adsorption Isotherms

Figures 8 (a and b) present the equilibrium adsorption data and the isotherm curves attained by fitting the results with four adsorption models. The corresponding parameters were calculated and summarized in Table 4. The q_{max} of M-GAC computed from the Langmuir isotherm for Mn(II) ions was 9.25 mg/g, which is 7.2 times greater than that of R-GAC (1.29 mg/g); the results suggest that the nitric acid treatment greatly enhanced the adsorption performance of M-GAC. The higher adsorption capacity is related mainly to the development of new carboxylic groups (-COOH) on M-GAC surface after modification process, consequently enhanced acidic dissociation and chelation in the cation exchange mechanism, forming surface complexes between Mn(II) ions and functional groups (ShamsiJazeyi and Kaghazchi, 2010; Rios *et al.,* 2003). The mechanism can be described as follows:

Dissociation step: $(\text{-COOH}) + H_2O \leftrightarrow (\text{-COO})^- + H_3O^+$
Chelation step: $2(\text{-COO})^- + Mn^{+2} \leftrightarrow (\text{-COO})_2Mn$

The linear regression coefficient (R^2) values of the four adsorption isotherms for M-GAC in Table 4 suggest that the best fit models were in the descending order of: Sips → Freundlich → Tempkin → Langmuir. Thus, Sips model is the most appropriate for representing the uptake behavior of Mn(II) on M-GAC. It is

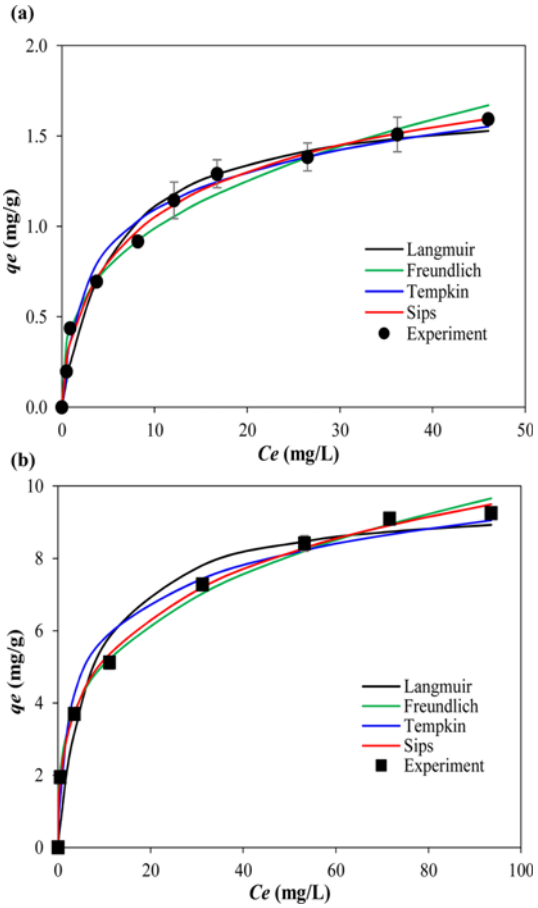

Fig. 8. Experimental Data and Nonlinearized Adsorption Isotherm Models at 25°C for Mn(II) Adsorption onto: (a) R-GAC, (b) M-GAC

Table 4. Isotherm Parameters for Mn(II) Adsorption onto R-GAC and M-GAC

Isotherm	Parameters		R-GAC	M-GAC
Langmuir	q_{max}	(mg/g)	1.29	9.25
	K	(L/mg)	0.39	0.57
	R^2		0.9848	0.9201
Freundlich	K_F	(mg/g (L/mg)$^{1/n}$)	0.33	2.47
	n		2.31	3.29
	R^2		0.9379	0.9960
Tempkin	b_T	(kJ/mol)	8.18	1.68
	A_T	(L/mg)	3.63	4.98
	R^2		0.9827	0.9673
Sips	q_{max}	(mg/g)	2.37	22.63
	K_s	(1/mg)	0.19	0.12
	n_s		0.62	0.40
	R^2		0.9936	0.9989

reasonable to consider that the M-GAC owns an energetically heterogeneous surface (i.e., a non-uniform surface) (Arshadi *et al.,* 2014). It is noteworthy that the Sips model is developed from the basis of the Freundlich and Langmuir models, which are

Table 5. Parameters of Kinetic Models Applied to Mn(II) Adsorption onto R-GAC and M-GAC

Model	Parameters		R-GAC	M-GAC
Pseudo first order	q_e	(mg/g)	1.54	8.99
	k_1	(1/min)	0.05	0.06
	R^2		0.9599	0.9959
Pseudo second order	q_e	(mg/g)	1.98	10.81
	k_2	(g/mg min)	0.01	0.02
	R^2		0.9936	0.9987
Intraparticle diffusion	k_{id}	(mg/g min$^{0.5}$)	0.20	1.53
	R^2		0.9979	0.9958
Three-stage model	ξ_1		0.002	0.010
	ξ_2		0.998	0.987
	α	(1/min)	0.012	0.125
	β		0.290	0.958
	γ		0.028	0.006
Mass transfer factor	B	(mg/g)	-0.53	-0.54
	δ	(g min/mg)	2.37	0.45
	R^2		0.9784	0.9695

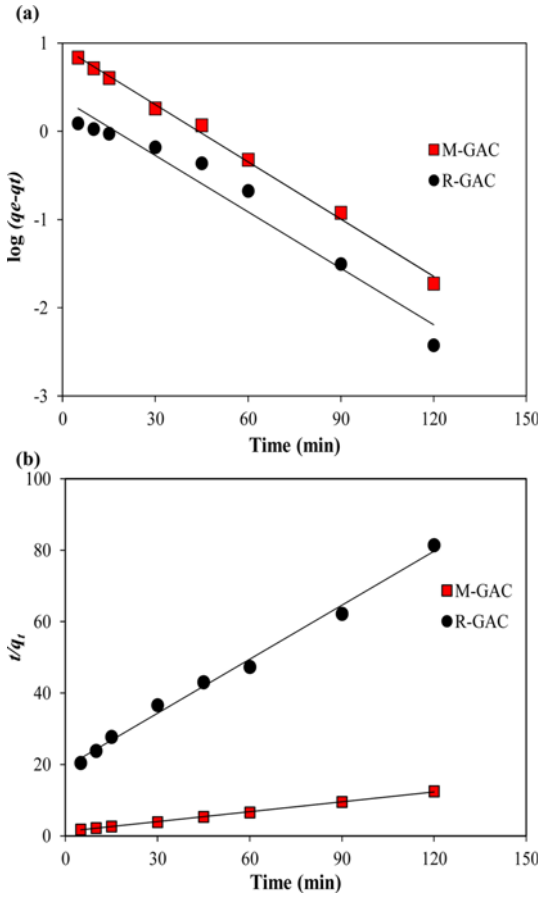

Fig. 9. Kinetic Models Applied to Mn(II) Adsorption for R-GAC and M-GAC at 25°C: (a) Pseudo First Order Model, (b) Pseudo Second Order Model

described by the dimensionless heterogeneity factor n_s. At values of n_s close to (or exactly) 1, the Sips isotherm approaches to the

Langmuir isotherm, which suggests a homogeneous adsorption. From Table 4, it was found that the value of n_s decreased from 0.62 for R-GAC to 0.40 for M-GAC, indicating that Mn(II) adsorption is more heterogeneous with M-GAC than with R-GAC (Kim *et al.,* 2016).

3.4 Adsorption Kinetics

Figures 9 (a and b) show the linearized forms of the pseudo first order and pseudo second order kinetic models, respectively, applied to experimental Mn(II) adsorption data obtained from M-GAC and R-GAC. The correlation coefficients (R^2) in Table 5 along with the fitting lines in Fig. 9 revealed that the pseudo second order model is more suitable than the pseudo first order model for both M-GAC and R-GAC, indicating that Mn(II) adsorbed onto both adsorbents are controlled by a chemisorption step. This result is expected, because we believe that kinetic behavior cannot simply be conceded as a reversible metal ions exchange occurring between the liquid and solid phases. Our results are consistent with previous adsorption studies using different carbon-based adsorbents for the uptake of heavy metal ions (Yi *et al.,* 2016; Mobasherpour *et al.,* 2014; Arshadi *et al.,* 2014). Additionally, the rate constant of M-GAC obtained from pseudo second order model is greater than that of R-GAC (Table 5), suggesting that M-GAC might have faster kinetic adsorption of aqueous Mn(II).

Figure 10 shows that the graph of q_t versus $t^{0.5}$ demonstrates multi-linearity correlations for both M-GAC and R-GAC, implying that multi kinetic stage govern the adsorption process (Vaghetti *et al.,* 2009). In addition, the data in Fig. 10 and Table 5 indicate that intraparticle diffusion was embarked on the rate limiting step, but it was not the sole one of the adsorption process due to the graphs did not go through the origin ($I \neq 0$) (Fig. 10) (Do and Kang, 2016). Indeed, the plot involves three linear fractions with different slopes, corresponding to three stages in the Mn(II) adsorption process by M-GAC. The first sharp portion is caused by external mass transfer, that Mn(II) ions diffused from bulk solution across the boundary layer to the exterior sites and macropores (film diffusion). Next, the intermediate linearized section is ascribed to the pore diffusion of Mn(II) ions from exterior sites to the micropores (intraparticle diffusion). Finally, the third plateau portion represents the intraparticle diffusion of Mn(II) ions begins to decelerate due to very low concentration of Mn(II) in the system (ShamsiJazeyi and Kaghazchi, 2010; Daifullah *et al.,* 2007). The graph in Fig. 10 reflects the dual nature of R-GAC, where an initial linear region of the curve pursued by a plateau region. It is noteworthy that the first (sharp) portion seems to be absent, suggesting that the external surface adsorption of Mn(II) ions occurs rapidly, and that the adsorption process rapidly progresses to the intraparticle diffusion stage (Omri *et al.,* 2016). We found that rapid adsorption occurred during the first stage with M-GAC; hence, it contributed significantly to the Mn(II) adsorption capacity. We believe that the faster kinetic adsorption of Mn(II) by M-GAC is largely due to the external surface sites, which were significantly changed after nitric acid treatment.

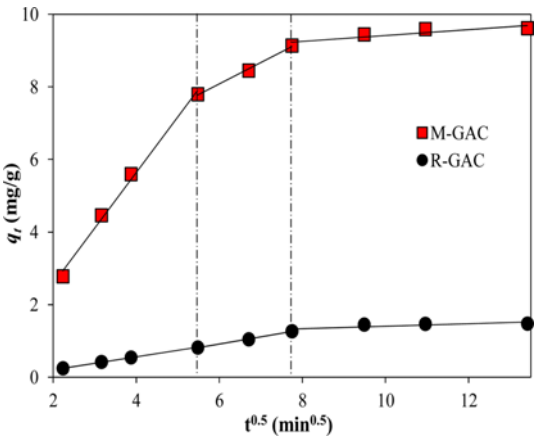

Fig. 10. Intraparticle Diffusion Model Applied to Mn(II) Adsorption onto R-GAC and M-GAC at 25°C

The three-stage kinetic model was used to provide additional evidence on the change of equilibrium adsorption behavior of Mn(II) on the exterior and interior adsorptive sites of the absorbents. These model parameters are summarized in Table 5. We found that the mass transfer rate constant of Mn(II) from the aqueous solution to the interior sites (α) of M-GAC is much higher than that of R-GAC, implying that M-GAC has faster kinetic adsorption of aqueous Mn(II). This is suitable with the data obtained from the pseudo second order model (discussed above). Also, a relative decrease in the instantaneous adsorption portion (ξ_1) compared to the interior adsorption portion (ξ_2) was observed for both M-GAC and R-GAC. This suggests that a major part of adsorption at infinite time occurred on the internal surface of both adsorbents (Choi *et al.,* 2007). It is noteworthy that the ξ_1 value of M-GAC was five times higher than that of R-GAC, indicating that nitric acid treatment enhanced Mn(II) adsorption on the external surface of M-GAC. Additionally, despite similar ξ_2 values, a higher limiting factor of the potential internal adsorption (β) at infinity was obtained for M-GAC; this results in a 3.3-fold rise in Mn(II) amount uptake at the interior adsorptive sites ($\beta\xi_2$) compared to that of R-GAC. These obtained results suggest that the nitric acid modification changed both the external and internal surfaces of M-GAC, which significantly changed the kinetic adsorption behavior and led to enhanced adsorption of Mn(II).

The mass transfer factor model was also applied to determine the resistance of mass transfer for the kinetic adsorption of Mn(II) ions from aqueous solution to the absorbents. The curves of plotting q against $\ln(t)$ show good linear regression coefficients (R^2), suggests that the parameters B and δ can be used to describe the mass transfer potential and the adsorbate-adsorbent affinity for the adsorption of Mn(II) ions, respectively (Table 5) (Fulazzaky *et al.*, 2017). The graphs of mass transfer factors (i.e., $[k_La]_g$, $[k_La]_f$ and $[k_La]_d$) versus C_t/C_o predicting the rates of GMF, EMT and IMT are presented in Fig. 11 (a and b). We observed that the variation of $[k_La]_g$, $[k_La]_f$ and $[k_La]_d$ values for M-GAC

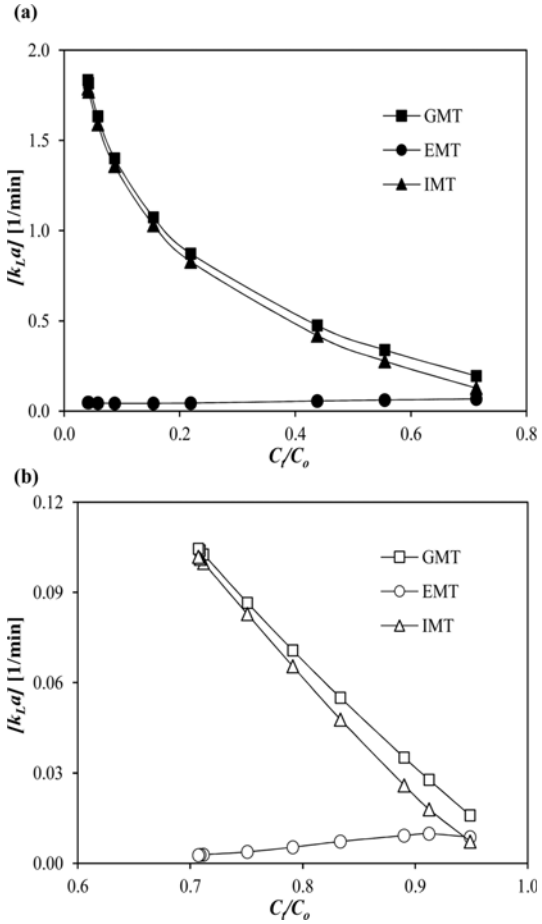

Fig. 11. Global Mass Transfer (GMT – $[k_La]_g$), External Mass Transfer (EMT – $[k_La]_f$) and Internal Mass Transfer (IMT – $[k_La]_d$) Factor Against C_t/C_o ratio of Mn(II) Adsorption onto: (a) M-GAC, (b) R-GAC

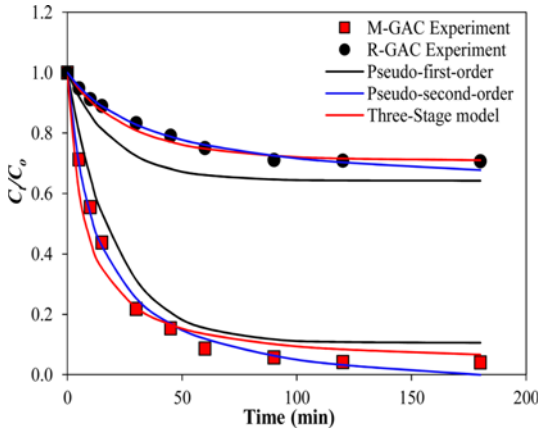

Fig. 12. Model Fits of Mn(II) Kinetic Adsorption onto R-GAC and M-GAC

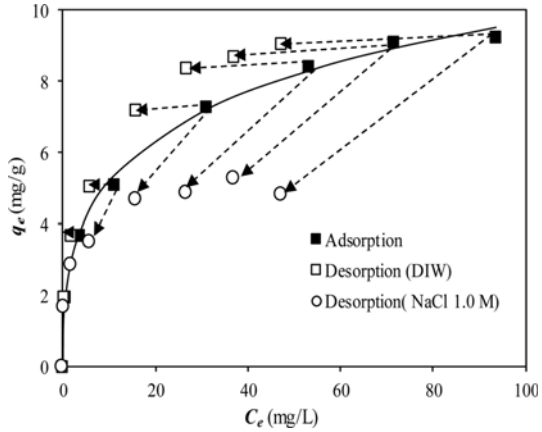

Fig. 13. Mn(II) Adsorption/desorption from M-GAC to Aqueous Solution

are all significantly higher than those of R-GAC, which can be ascribed to a greater in the adsorbate-adsorbent affinity of M-GAC to attract Mn(II) ions (Fulazzaky, 2011). It is consistent with the above results that there is a chemisorption, by which the covalent bonding between the Mn(II) ions and acidic carboxylic functional groups on the surface of M-GAC encourages the increase of attractive forces between the adsorbate and adsorbent (Fulazzaky, 2011). In addition, we found a very similar in the trend and variation of the IMT rate ($[k_La]_d$) compared to the GMF rate ($[k_La]_g$) for both absorbents. Also, the values of $[k_La]_d$ are much higher than the values of $[k_La]_f$ represented the EMT rate, indicating that the resistance of mass transfer is dependent on the external mass transfer (Fulazzaky *et al.*, 2017).

Validation of four adsorption kinetic models mentioned above with the experimental data is provided in Fig. 12. As can be seen, the three-stage model is the most appropriate for representing the kinetic adsorption of Mn(II) ions for both M-GAC and R-GAC.

3.5 Desorption

Figure 13 presents the desorption of Mn(II) by using different eluents (i.e., DIW and NaCl 1.0 M). The result shows that a negligible amount of Mn(II) was detached from the M-GAC surface (less than 5%) during the desorption process using DIW as an eluent. This is consistent with our observation that chemisorption takes places on the M-GAC surface, which is predominantly irreversible or has extremely slow liberation process; thus, desorption does not proceed easily by DIW. In addition, we observed no considerable differences in the amount of desorbed Mn(II) by DIW at varying temperatures (data not shown), implying that the effect of solution temperature (20 – 40°C) on the desorption of Mn(II) ions is insignificant. However, high level of Mn(II) (above 51%) was liberated from the M-GAC surface during the desorption process with NaCl 1.0 M, indicating that the adsorption of Mn(II) is controlled by ion exchange (Huang *et al.*, 2009). These results suggested Mn(II) can be easily desorbed under suitable conditions without destroying the M-GAC structure for subsequent reuse. Further study is needed to find out an effective desorbing agent, which is cheap, non-polluting and non-damaging the structure of M-GAC.

4. Conclusions

In this work, M-GAC showed an improvement in its porous structure after nitric acid modification. Also, acid treatment resulted in a lower pH_{PZC} and more surface carboxylic acid groups. The uptake of Mn(II) ions was dramatically influenced by experimental conditions, i.e., pH solution, initial Mn(II) concentration, adsorbent dose, and temperature. The adsorption behavior of Mn(II) ions onto M-GAC and R-GAC can be explained well using Sips isotherm model. The q_{max} of Mn(II) by M-GAC was increased by 7.2 times compared with R-GAC, and an increase in the heterogeneity of the adsorption was also observed. The pseudo second order kinetic model was appropriate for fitting the experimental data of both M-GAC and R-GAC. Furthermore, the three-stage kinetic model validated that acid treatment significantly changed the surface properties of M-GAC, resulting in 5.0- and 3.3-fold increases in the quantity of Mn(II) ions uptake on the external and internal surfaces, respectively, compared to those of R-GAC. In addition, the rate-limiting step consists of both external mass transfer and intraparticle diffusion for the uptake of Mn(II) by M-GAC. Finally, the mass transfer factor model verified that the mass transfer resistance for the adsorption of Mn(II) onto M-GAC is mainly dependent on the external mass transfer. Our results suggested that M-GAC can be easily prepared and employed as an effective industrial absorbent to collect heavy metals from water and wastewater.

Acknowledgements

This research was partially supported by the Korea Ministry of Environment (MOE) as a "Converging Technology Program", "GAIA (Geo-Advanced Innovative Action)" Project (#2015000550004), and by a Notional Research Foundation of Korea (NRF) grant (NRF-2016R1A2B4015385).

References

Ademiluyi, F. T. and David-West, E. O. (2012). "Effect of chemical activation on the adsorption of heavy metals using activated carbons from waste materials." *ISRN Chem. Eng.*, Vol. 2012, p. 5, DOI: 10.5402/2012/674209.

Ahn, C. K., Kim, Y. M., Woo, S. H., and Park, J. M. (2009). "Removal of cadmium using acid-treated activated carbon in the presence of nonionic and/or anionic surfactants." *Hydrometallurgy*, Vol. 99, Nos. 3-4, pp. 209-213, DOI: 10.1016/j.hydromet.2009.08.008.

Anisuzzaman, S. M., Joseph, C. G., Taufiq-Yap, Y. H., Krishnaiah, D., and Tay, V. V. (2015). "Modification of commercial activated carbon for the removal of 2,4-dichlorophenol from simulated wastewater." *J. King. Saud. Univ. Sci.*, Vol. 27, No. 4, pp. 318-330, DOI: 10.1016/j.jksus.2015.01.002.

Arshadi, M., Amiri, M. J., and Mousavi, S. (2014). "Kinetic, equilibrium and thermodynamic investigations of Ni(II), Cd(II), Cu(II) and Co(II) adsorption on barley straw ash." *Water Resour. Ind.*, Vol. 6, pp. 1-17, DOI: 10.1016/j.wri.2014.06.001.

Belaid, K. D., Kacha, S., Kameche, M., and Derriche, Z. (2013). "Adsorption kinetics of some textile dyes onto granular activated carbon." *J. Environ. Chem. Eng.*, Vol. 1, No. 3, pp. 496-503, DOI: 10.1016/j.jece.2013.05.003.

Bhatnagar, A., Hogland, W., Marques, M., and Sillanpää, M. (2013). "An overview of the modification methods of activated carbon for its water treatment applications." *Chem. Eng. J.*, Vol. 219, pp. 499-511, DOI: 10.1016/j.cej.2012.12.038.

ChangMing, D., DongWei, H., HongXia, L., MuDan, X., Kui, W., Lu, Z., ZhiYi, L., TengFei, C., JianMin, M., Dong, G., YuHao, H., ShangKun, L., Liao, Y., and ChuangRong, Z. (2013). "Adsorption of acid orange II from aqueous solution by plasma modified activated carbon fibers." *Plasma Chem. Plasma Process.*, Vol. 33, No. 1, pp. 65-82, DOI: 10.1007/s11090-012-9412-x.

Choi, J.-W., Choi, N.-C., Lee, S.-J., and Kim, D.-J. (2007). "Novel three-stage kinetic model for aqueous benzene adsorption on activated carbon." *J. Colloid Interf. Sci.*, Vol. 314, No. 2, pp. 367-372, DOI: 10.1016/j.jcis.2007.05.070.

Choy, K. K. H., McKay, G., and Porter, J. F. (1999). "Sorption of acid dyes from effluents using activated carbon." *Resour. Conserv. Recycl.*, Vol. 27, Nos. 1-2, pp. 57-71, DOI: 10.1016/S0921-3449(98)00085-8.

Do, Q. C. and Kang, S. (2016). "Thermodynamic analysis of fatty acid harvesting by novel carbon-based adsorbent." *Environ. Sci. Pollut. Res*, Vol. 23, No. 8, pp. 7146-7154, DOI: 10.1007/s11356-015-4428-4.

Do, Q. C., Kim, D.-G., and Ko, S.-O. (2017). "Nonsacrificial template synthesis of magnetic-based yolk–shell nanostructures for the removal of acetaminophen in fenton-like systems." *ACS Appl. Mater. Interfaces*, Vol. 9, No. 34, pp. 28508-28518, DOI: 10.1021/acsami.7b07658.

Emmanuel, K. A. and Rao, A. V. (2009). "Comparative study on adsorption of Mn(II) from aqueous solutions on various activated carbons." *E-J. Chem.*, Vol. 6, No. 3, pp. 693-704, DOI: 10.1155/2009/587159.

Freundlich, H. (1906). "Over the adsorption in solution." *J. Phys. Chem.*,Vol. 57, pp. 1100-1107.

Fulazzaky, M. A. (2011). "Determining the resistance of mass transfer for adsorption of the surfactants onto granular activated carbons from hydrodynamic column." *Chem. Eng. J.*, Vol. 166, No. 3, pp. 832-840, DOI: 10.1016/j.cej.2010.11.052.

Fulazzaky, M. A., Khamidun, M. H., and Omar, R. (2013). "Understanding of mass transfer resistance for the adsorption of solute onto porous material from the modified mass transfer factor models." *Chem. Eng. J.*, Vol. 228, pp. 1023-1029, DOI: 10.1016/j.cej.2013.05.100.

Fulazzaky, M. A., Majidnia, Z., and Idris, A. (2017). "Mass transfer kinetics of Cd(II) ions adsorption by titania polyvinylalcohol-alginate beads from aqueous solution." *Chem. Eng. J.*, Vol. 308, pp. 700-709, DOI: 10.1016/j.cej.2016.09.106.

Gaur, V. and Shankar, P. (2008). "Surface modification of activated carbon for the removal of water impurities." *Water. Cond. Purif.*, pp. 1-5.

Goel, J., Kadirvelu, K., Rajagopal, C., and Kumar Garg, V. (2005). "Removal of lead(II) by adsorption using treated granular activated carbon: Batch and column studies." *J. Hazard. Mater.*, Vol. 125, Nos. 1-3, pp. 211-220, DOI: 10.1016/j.jhazmat.2005.05.032.

Huang, G. L., Shi, J. X., and Langrish, T. A. G. (2009). "Removal of Cr(VI) from aqueous solution using activated carbon modified with nitric acid." *Chem. Eng. J.*, Vol. 152, Nos. 2-3, pp. 434-439, DOI: 10.1016/j.cej.2009.05.003.

Jaramillo, J., Álvarez, P. M., and Gómez-Serrano, V. (2010). "Preparation and ozone-surface modification of activated carbon. Thermal stability of oxygen surface groups." *Appl. Surf. Sci.*, Vol. 256, No. 17, pp. 5232-

5236, DOI: 10.1016/j.apsusc.2009.12.109.

Jia, Y. F. and Thomas, K. M. (2000). "Adsorption of cadmium ions on oxygen surface sites in activated carbon." *Langmuir*, Vol. 16, No. 3, pp. 1114-1122, DOI: 10.1021/la990436w.

Kim, D.-G., Nhung, T. T., and Ko, S.-O. (2016). "Enhanced adsorption of heavy metals with biogenic manganese oxide immobilized on zeolite." *KSCE J. Civ. Eng.*, Vol. 20, No. 6, pp. 2189-2196, DOI: 10.1007/s12205-016-0356-1.

Langmuir, I. (1918). "The adsorption of gases on plane surfaces of glass, mica and platinum." *J. Am. Chem. Soc.*, Vol. 40, No. 9, pp. 1361-1403, DOI: 10.1021/ja02242a004.

Li, Z., Imaizumi, S., Katsumi, T., Inui, T., Tang, X., and Tang, Q. (2010). "Manganese removal from aqueous solution using a thermally decomposed leaf." *J. Hazard. Mater.*, Vol. 177, Nos. 1-3, pp. 501-507, DOI: 10.1016/j.jhazmat.2009.12.061.

Michalke, B. and Fernsebner, K. (2014). "New insights into manganese toxicity and speciation." *J. Trace Elem. Med. Biol.*, Vol. 28, No. 2, pp. 106-116, DOI: 10.1016/j.jtemb.2013.08.005.

Mobasherpour, I., Salahi, E., and Ebrahimi, M. (2014). "Thermodynamics and kinetics of adsorption of Cu(II) from aqueous solutions onto multi-walled carbon nanotubes." *J. Saudi Chem. Soc.*, Vol. 18, No. 6, pp. 792-801, DOI: 10.1016/j.jscs.2011.09.006.

Omri, A., Wali, A., and Benzina, M. (2016). "Adsorption of bentazon on activated carbon prepared from Lawsonia inermis wood: Equilibrium, kinetic and thermodynamic studies." *Arabian J. Chem.*, Vol. 9, pp. S1729-S1739, DOI: 10.1016/j.arabjc.2012.04.047.

Patil, D. S., Chavan, S. M., and Oubagaranadin, J. U. K. (2016). "A review of technologies for manganese removal from wastewaters." *J. Environ. Chem. Eng.*, Vol. 4, No. 1, pp. 468-487, DOI: 10.1016/j.jece.2015.11.028.

Rios, R. R. A., Alves, D. E., Dalmázio, I., Bento, S. F. V., Donnici, C. L., and Lago, R. M. (2003). "Tailoring activated carbon by surface chemical modification with O, S, and N containing molecules." *Mater. Res.*, Vol. 6, No. 2 pp. 129-135.

Rivera-Utrilla, J., Sánchez-Polo, M., Gómez-Serrano, V., Álvarez, P. M., Alvim-Ferraz, M. C. M., and Dias, J. M. (2011). "Activated carbon modifications to enhance its water treatment applications. An overview." *J. Hazard. Mater.*, Vol. 187, Nos. 1-3, pp. 1-23, DOI: 10.1016/j.jhazmat.2011.01.033.

Robati, D. (2013). "Pseudo-second-order kinetic equations for modeling adsorption systems for removal of lead ions using multi-walled carbon nanotube." *J. Nanostructure Chem.*, Vol. 3, No. 55, pp. 1-6, DOI: 10.1186/2193-8865-3-55.

ShamsiJazeyi, H. and Kaghazchi, T. (2010). "Investigation of nitric acid treatment of activated carbon for enhanced aqueous mercury removal." *J. Ind. Eng. Chem.*, Vol. 16, No. 5, pp. 852-858, DOI: 10.1016/j.jiec.2010.03.012.

Sips, R. (1948). "On the structure of a catalyst surface." *J. Chem. Phys.*, Vol. 16, No. 5, pp. 490-495.

Tavlieva, M. P., Genieva, S. D., Georgieva, V. G., and Vlaev, L. T. (2015). "Thermodynamics and kinetics of the removal of manganese(II) ions from aqueous solutions by white rice husk ash." *J. Mol. Liq.*, Vol. 211, pp. 938-947, DOI: 10.1016/j.molliq.2015.08.015.

Üçer, A., Uyanik, A., and Aygün, Ş. F. (2006). "Adsorption of Cu(II), Cd(II), Zn(II), Mn(II) and Fe(III) ions by tannic acid immobilised activated carbon." *Sep. Purif. Technol.*, Vol. 47, No. 3, pp. 113-118, DOI: 10.1016/j.seppur.2005.06.012.

Vaghetti, J. C. P., Lima, E. C., Royer, B., da Cunha, B. M., Cardoso, N. F., Brasil, J. L., and Dias, S. L. P. (2009). "Pecan nutshell as biosorbent to remove Cu(II), Mn(II) and Pb(II) from aqueous solutions." *J. Hazard. Mater.*, Vol. 162, No. 1, pp. 270-280, DOI: 10.1016/j.jhazmat.2008.05.039.

Weber, W. J. and Morris, J. C. (1963). "Kinetics of adsorption on carbon from solution." *J. Sanit. Eng. Div.*, Vol. 89, No. 2, pp. 31-60.

WHO (2011). *Manganese in Drinking-Water. Background Document for of WHO Guidelines for Drinking-Water Quality*, World Health Organization. Geneva. (WHO/SDE/WSH/03.04/104/Rev/1).

Yahya, M. A., Al-Qodah, Z., and Ngah, C. W. Z. (2015). "Agricultural bio-waste materials as potential sustainable precursors used for activated carbon production: A review." *Renew. Sustainable Energy Rev.*, Vol. 46, pp. 218-235, DOI: 10.1016/j.rser.2015.02.051.

Yang, L., Huang, T., Jiang, X., Li, J., and Jiang, W. (2016). "The effects of metal oxide blended activated coke on flue gas desulphurization." *RSC Adv.*, Vol. 6, pp. 55135-55143, DOI: 10.1039/C6RA05407B.

Yi, Z., Yao, J., Zhu, M., Chen, H., Wang, F., and Liu, X. (2016). "Kinetics, equilibrium, and thermodynamics investigation on the adsorption of lead(II) by coal-based activated carbon." *SpringerPlus*, Vol. 5, No. 1160, pp. 1-12, DOI: 10.1186/s40064-016-2839-4.

Zhang, G., Shi, L., Zhang, Y., Wei, D., Yan, T., Wei, Q., and Du, B. (2015). "Aerobic granular sludge-derived activated carbon: mineral acid modification and superior dye adsorption capacity." *RSC Adv.*, Vol. 5, pp. 25279-25286, DOI: 10.1039/C4RA15216F.